Institute of Space and Aeronautical Science, University of Tokyo
Report No. 572, July 1979

A Kinetic Approach to Non-linear Condensation and/or Evaporation Processes

By

Masayuki HATAKEYAMA* and Hakuro OGUCHI

Summary: This paper concerns with the non-linear steady condensation and/or evaporation processes of pure vapor flowing along an infinitely plane wall. The aim is to analyze these processes by means of an extended two-stream moment method for a wide variety of flow parameters, and to clarify the dependence of the processes on various flow parameters with or without mean parallel velocity. The condensation rate depends, in general, on the ambient, uniform flow parameters (density, pressure or temperature, and mean parallel velocity), while for smaller condensation rates it depends on the pressure alone. The evaporation rate depends on the ambient pressure alone for any rate and the solution is achieved only for the cases without the mean parallel velocity. As regards the effect of the mean parallel velocity on the condensation rate, the rate indicates pronounced decrease with increasing the mean parallel velocity. For the Couette flow, the effect of the mass flux on the flow behavior is also clarified.

I. INTRODUCTION

In the present paper, we are concerned with the non-linear steady condensation and/or evaporation processes of pure vapor flowing along an infinitely plane wall and also flowing between the two parallel plates with or without mean parallel velocity.

For simplicity, first suppose the half space problem of condensation which takes place on an infinitely plane interphase. The problem on condensation was analyzed based on the free molecule theory by Hertz [*1*] and Knudsen [*2*], and thereafter by Schrage [*3*] with some improvements. According to these analyses, the mass flux can be determined for any temperatures and pressures specified at the boundaries; that is, both on the interphase and at the infinitely far region.

In the past decade, a number of analyses on the problem of condensation and/or evaporation have been progressed on the basis of the kinetic theory. In a linearized version, the analysis was made by several authors [*5–8*]. In an ordinary linearization of the problem, the heat flux normal to the interphase may be neglected as the higher-order small quantity. With no heat-flux, however, the solution is obtained only for the selected values of temperatures and pressures at the boundaries [*6–8*]. With the heat flux retained, for the condensation problem the solution can be achieved for any specified temperatures and pressures at the boundaries [*5, 15*]. This implies that the condensation problem must be dealt with from a non-linear version.

The half space problem with or without the mean parallel velocity was analyzed by

* Tokyo Metropolitan College of Aeronautical Engineering.

Kogan and Makashev [9] on the basis of the non-linear BGK model equation. The flow structure and the relevant characteristic quantities were presented for several numerical examples. Gajewski *et al.* [10] also presented some numerical examples under a restricted flow condition without the mean parallel velocity. Since, however, the analysis of the non-linear problem necessarily relies on numerical computations, a number of examples so far presented are unlikely to be sufficient to provide the full understanding of the problem.

In the half space problem, the evaporation problem involves some different features from the condensation problem. As pointed out in the literatures [9, 11, 12], the solution for the problem can be achieved only for flows without the mean parallel velocity, along with the selected values of temperatures and pressures at the boundaries.

For both the two-surface and the Couette flow problems, the similar analysis was made by Makashev [13]. More recently for the two-surface problem Yen [14] solved the Boltzmann equation by the Monte-Carlo method. As regards the two-surface problem, the ordinary linearization leads to no restricted solution [8], because the heat flux retains finite on the contrast to that in the half space condensation problem. On the aforementioned fact it can be said that the linearized analysis provides a proper understanding of the two-surface problem for the case of smaller mass flux.

In view of the present status above reviewed, we aim to perform the non-linear analysis of the flow structure with condensation and/or evaporation over a wide variety of flow parameters and also focus a particular attention on the dependence of condensation processes on various flow parameters with or without the mean parallel velocity. To achieve the present aim, a simple but comparatively accurate method of analysis is developed on the basis of the two-stream Maxwellian moment method primarily proposed by Lees [4].

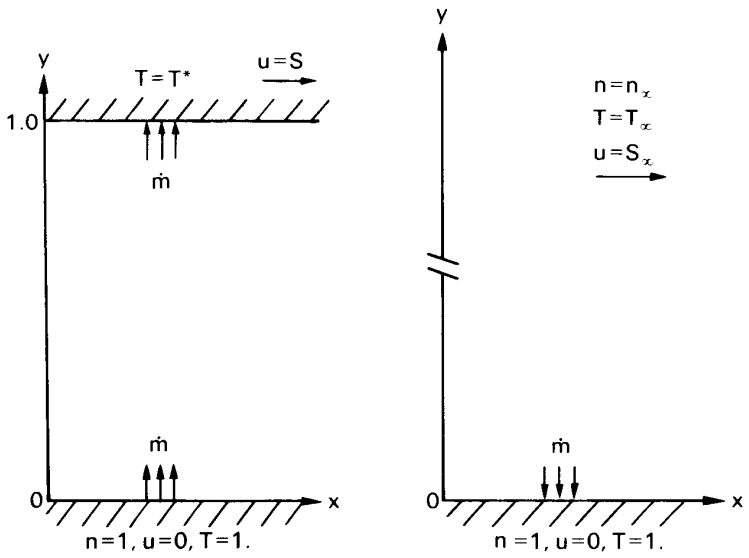

1a. Couette Flow 1b. Half Space Flow

FIG. 1. Sketch of flow configurations.

II. Mathematical Formulation

We consider one dimentional, steady vapor flows in the absence of external forces. A sketch of flow field is shown in Fig. 1; the Couette flow and the half space flow. For the Couette flow case, Fig. 1a, the vapor evaporates out of the lower interphase at $y=0$, and condenses onto the upper interphase at $y=1$. For the half space flow case, Fig. 1b, the vapor condenses onto the interphase at $y=0$. It is assumed that no reaction occurs in the gas phase. The gas molecules are assumed to be the Maxwell molecule model whose intermolecular force F is defined as follows;

$$F = m^2 \frac{K}{r^5},$$

where m is the molecular mass, K is the force constant, and r is the distance between molecules. The Maxwell-Boltzmann transport equation is written using the standard symbols as

$$\frac{d}{dy}\int V_y \varphi f d\boldsymbol{V} = \int (\varphi' - \varphi) f f_1 g b db d\varepsilon d\boldsymbol{V} d\boldsymbol{V}_1, \tag{2.1}$$

where φ is any function of the molecular velocity $\boldsymbol{V}$, and the primed φ' denotes the function of $\boldsymbol{V}$ after the collision. Apparently, in the moment method, the accuracy of the solution depends on the choice of the explicit form of φ. The second- or third-order functions of $\boldsymbol{V}$ together with the four collisional invariants $(1, V_x, V_y, V^2)$ may be chosen; for example, V_xV_y, V_x^2, V_y^2, V_x^3, V_y^3, V^2V_x and V^2V_y are selected as the transport quantities. To hold the accuracy of the approximation of the moment equations, the φ is usually selected under the criterion that a priority should be given to the lower order φ (i.e. lower order moment equation) and to the φ in the direction normal to the wall (for example, V_y^2).

In the present analysis, the two-stream Maxwellian velocity distribution function $f_\pm$ is assumed for the form of the solution $f(y, \boldsymbol{V})$ in Eq. (2.1). In this method, the velocity space $\boldsymbol{V}$ is divided into two half velocity space, $V_y>0$ and $V_y<0$, and the half range Maxwellian distribution functions containing four unknown functions for each half velocity space are assumed;

$$f(y,\boldsymbol{V}) = f_+(y,\ \boldsymbol{V};\ V_y>0) + f_-(y,\ \boldsymbol{V};\ V_y<0)$$

$$f_\pm = \frac{n_\pm(y)}{\pi^{3/2}c_\pm(y)^3} \exp\left[-\frac{(\boldsymbol{V} - \boldsymbol{v}_\pm(y))^2}{c_\pm(y)^2}\right],$$

$$\boldsymbol{u}_\pm(y) = (u_\pm(y),\ v_\pm(y),\ 0),$$

$$c_\pm(y) = (2RT_\pm(y))^{1/2}.$$

For convenience, all the variables are non-dimensionarized; that is, the temperature T is referred to the T_w at the lower wall ($y=0$), the number density n to the saturated number density n_w corresponding to T_w, the velocities $(\boldsymbol{V}, \boldsymbol{u}_\pm, v_\pm)$ to the thermal velocity c_w $(=(2RT_w)^{1/2})$, and y-coordinate to the mean free path λ_w for the half space

flow case and to the width D between two parallel walls for the Couette flow case. The λ_w for the Maxwell molecule model is

$$\lambda_w = (kT_w)^{1/2}/[3A_2(5)(\pi K)^{1/2} m n_w]$$

The Knudsen number for the Couette flow case is defined as $Kn = \lambda_w/D$. In what follows, we shall employ the same symbols as the dimensional variables for the non-dimensionarized variables unless otherwise stated.

By using the two-stream distribution function $f_\pm$, the n-th order moments are defined as follows:

$$M^{(n)}_{\alpha_1\alpha_2\cdots\alpha_N} = \int \prod_{\beta=1}^{n} V_{\alpha_\beta} f_\pm dV,$$

$$\mathcal{M}^{(n)}_{\alpha_1\alpha_2\cdots\alpha_N} = \int \prod_{\beta=1}^{n} (V_{\alpha_\beta} - u_{\alpha_\beta}) f_\pm dV, \tag{2.2}$$

where

$$\int \prod_{\beta=1}^{n} V_{\alpha_\beta} f_\pm \, dV = \int_{(V_{\alpha_\beta}>0)} \prod_{\beta=1}^{n} V_{\alpha_\beta} f_+ \, dV + \int_{(V_{\alpha_\beta}<0)} \prod_{\beta=1}^{n} V_{\alpha_\beta} f_- \, dV.$$

The macroscopic flow quantities are expressed using the n-th order moment as follows:

$$\begin{aligned} n(y) &= M^{(0)} \\ u(y) &= \frac{M^{(1)}_x}{n} \\ v(y) &= \frac{M^{(1)}_y}{n} \\ T(y) &= \frac{2}{3n}\left(\mathcal{M}^{(2)}_{xx} + \mathcal{M}^{(2)}_{yy} + \mathcal{M}^{(2)}_{zz}\right) \\ p(y) &= nT \\ \dot{q}_y(y) &= \frac{1}{2}\left(\mathcal{M}^{(3)}_{xxy} + \mathcal{M}^{(3)}_{yyy} + \mathcal{M}^{(3)}_{yzz}\right) \end{aligned} \tag{2.3}$$

where $\dot{q}_y(y)$ is the heat flux normal to the wall. The two-stream moment equations generated are listed up as follows:

(1) $\varphi = 1$ (mass conservation)

$$\begin{aligned} & M^{(1)}_{xy} = Z_0, \\ \text{or} \quad & n_+ c_+ K^{(1)} + n_- c_- L^{(1)} = Z_0 . \end{aligned} \tag{2.4}$$

(2) $\varphi = V_x$ (momentum conservation parallel to wall)

$$M_{xy}^{(2)} = Z_1,$$

$$\text{or} \qquad n_+ c_+ u_+ K^{(1)} + n_- c_- u_- L^{(1)} = Z_1 . \tag{2.5}$$

(3) $\varphi = V_y$ (momentum conservation normal to wall)

$$M_{yy}^{(2)} = Z_2,$$

$$\text{or} \qquad n_+ c_+^2 K^{(2)} + n_- c_-^2 L^{(2)} = Z_2 . \tag{2.6}$$

(4) $\varphi = V^2$(energy conservation)

$$M_{\alpha_i \alpha_i y}^{(3)} = Z_3,$$

$$\text{or} \qquad n_+ c_+^3 [(1 + u_+^2/c_+^2) K^{(1)} + K^{(3)}]$$

$$+ n_- c_-^3 [(1 + u_-^2/c_-^2) L^{(1)} + L^{(3)}] = Z_3 . \tag{2.7}$$

where $K^{(1)}$, $K^{(2)}$, $K^{(3)}$ and $K^{(4)}$ are the functions with respect to v_+/c_+, and $L^{(1)}$, $L^{(2)}$, $L^{(3)}$ and $L^{(4)}$ are the functions with respect to v_-/c_-. The table of contents for these functions is presented in Appendix. The Z_0, Z_1, Z_2 and Z_3 are the conservation fluxes. For the transport quantities the following moment equations are derived;

(5) $\varphi = V_x V_y$

$$\frac{d}{dy} M_{xyy}^{(3)} = -\frac{3}{4Kn} (M_x^{(1)} M_y^{(1)} - M^{(0)} M_{xy}^{(2)}),$$

(6) $\varphi = V_y^2$

$$\frac{d}{dy} M_{yyy}^{(3)} = \frac{1}{4Kn} (2(M_y^{(1)})^2 - 3M^{(0)} M_{yy}^{(2)} + M^{(0)} M_{\alpha_i \alpha_i}^{(2)} - (M_x^{(1)})^2),$$

(7) $\varphi = V_x^2$

$$\frac{d}{dy} M_{xxy}^{(3)} = \frac{1}{4Kn} (2(M_x^{(1)})^2 - 3M^{(0)} M_{xx}^{(2)} + M^{(0)} M_{\alpha_i \alpha_i}^{(2)} - (M_y^{(1)})^2),$$

(8) $\varphi = V_y^3$

$$\frac{d}{dy} M_{yyyy}^{(4)} = \frac{3}{8Kn} (M_y^{(1)} M_{yy}^{(2)} + M_y^{(1)} M_{\alpha_i \alpha_i}^{(2)} + M^{(0)} M_{\alpha_i \alpha_i y}^{(3)}$$

$$- 3M^{(0)} M_{yyy}^{(3)} - 2M_x^{(1)} M_{xy}^{(2)}),$$

(9) $\varphi = V_x^3$

$$\frac{d}{dy} M_{xxxy}^{(4)} = \frac{3}{8Kn} (M_x^{(1)} M_{xx}^{(2)} + M_x^{(1)} M_{\alpha_i \alpha_i}^{(2)} + M^{(0)} M_{\alpha_i \alpha_i x}^{(3)}$$

$$- 3M^{(0)} M_{xxx}^{(3)} - 2M_y^{(1)} M_{xy}^{(2)}),$$

(10) $\varphi = V^2 V_y$

$$\frac{d}{dy} M^{(4)}_{\alpha_i \alpha_i yy} = \frac{1}{2Kn}(2M^{(1)}_y M^{(2)}_{\alpha_i \alpha_i} - M^{(1)}_y M^{(2)}_{yy} - M^{(0)} M^{(3)}_{\alpha_i \alpha_i y} - M^{(1)}_x M^{(2)}_{xy}),$$

(11) $\varphi = V^2 V_x$

$$\frac{d}{dy} M^{(4)}_{\alpha_i \alpha_i xy} = \frac{1}{2Kn}(2M^{(1)}_x M^{(2)}_{\alpha_i \alpha_i} - M^{(1)}_x M^{(2)}_{xx} - M^{(0)} M^{(3)}_{\alpha_i \alpha_i x} - M^{(1)}_y M^{(2)}_{xy}).$$

It should be noted that the repeated subscript $\alpha_i \alpha_i$ means the summation and that the Knudsen number is equal to unity for the half space flow case. With regard to the detailed derivation of the above moment equations, Ref. 16 should be referred to.

As for the boundary conditions, the distribution function f_+ for the molecules emitting out of the interphase is assumed to be the Maxwellian distribution function with the temperature of the interphase T_w, and the saturated number density n_w corresponding to T_w. That is, the fully diffuse reemission distribution function is assumed, and the evaporation coefficient α_e is unity. It is assumed that all the molecules coming onto the interphase are absorbed. That is, the condensation coefficient α_c is also unity. At the lower boundary,

$$n_+(0) = 1,\ u_+(0) = 0,\ v_+(0) = 0,\ c_+(0) = 1. \tag{2.8}$$

At the upper boundary for the Couette flow case,

$$u_-(1) = S,\ v_-(1) = 0,\ c_-(1) = T^*, \tag{2.9}$$

where S is the speed ratio. The boundary condition for $n_-(1)$ is not given explicitly in Eq. (2.9). There are two schemes to set the boundary condition for $n_-(1)$. The first scheme is to give the evaporation mass flux $\dot{m}$ as the free parameter instead of $n_-(1)$. The $n_-(1)$ is obtained by solving the mass conservation equation

$$n_+ c_+ K^{(1)} + n_- c_- L^{(1)} = \dot{m}.$$

The second scheme is to give $n_-(1)$ explicitly through the Clausius-Clapeyron formula with the parameter $\beta(=Q/RT)$, where Q is the specific latent heat and is assumed constant:

$$n_-(1) = \frac{1}{T^*} \exp\,[\beta(1 - 1/T^*)].$$

We use the evaporation mass flux rate $\dot{m}$ as the flow parameter for the Couette flow case to simplify the numerical procedures which are described in the next section.

At infinity, for the half space flow case, the flow approaches to equilibrium with the velocity $\boldsymbol{u}_\infty(=(S_\infty, v_\infty, 0))$ and the temperature T_∞. In other words, the distribution function f_+ tends to the full range Maxwellian distribution function. Therefore we have

$$n_+(\infty) = n_-(\infty) = n_\infty, \qquad u_+(\infty) = u_-(\infty) = S_\infty,$$
$$v_+(\infty) = v_-(\infty) = v_\infty, \qquad c_+(\infty) = c_-(\infty) = T_\infty^{1/2}, \tag{2.10}$$

where the v_∞ is obtained as the result of the calculation, and the number density n_∞ is given by the following formula;

$$n_\infty = \frac{1}{T_\infty} \exp\left(\beta(1 - 1/T_\infty)\right), \qquad \beta = \frac{\ln(n_\infty T_\infty)}{(1 - 1/T_\infty)}, \tag{2.11}$$

which have the same form of the Clausius-Clapeyron formula. Equation (2.11) is used as a convenient formula to give the number density n_∞. When Eq. (2.11) is linearized under the assumption of the slight deviation from equilibrium, the following simple formula is obtained;

$$n_\infty = 1 + \beta_l(T_\infty - 1), \qquad \beta_l = \frac{(n_\infty - 1)}{(T_\infty - 1)}. \tag{2.12}$$

which are often used in the linearized analyses [5]–[8].

A. A simple analysis in the linearized flow regime for the half space flow case

First we consider the linearized case, in which all the quantities are slightly deviated from equilibrium values; that is, $n_\pm = 1 + \Delta n_\pm$, $c_\pm = 1 + \Delta c_\pm$, and then $|\Delta n_\pm| \ll 1$, $|\Delta c_\pm| \ll 1$, and $|v_\pm| \ll 1$. For simplicity we consider the cases of vanishing mean parallel velocity or $S_\infty = 0$. The boundary conditions for $\Delta n_\pm$, $\Delta c_\pm$, $v_\pm$, are as follows:

$$\begin{aligned} &\text{at } y = 0; \qquad \Delta n_+ = 0,\ v_+ = 0,\ \Delta c_+ = 0. \\ &\text{at } y \to \infty; \qquad \Delta n_+ = \Delta n_- = (n_\infty - 1),\ v_+ = v_- = v_\infty,\ \Delta c_+ = \Delta c_- = (T_\infty - 1) \end{aligned} \tag{2.13}$$

Using Eq. (2.13), the conservation equations (2.4–2.7) are applied to the conditions at the interphase and at infinity:

$$Z_0 = -(\Delta n_-(0) + \Delta c_-(0))/(2\pi^{1/2}) = v_-(0)/2 = v_\infty,$$
$$Z_2 = 1/2 + (\Delta n_-(0) + 2\Delta c_-(0))/4 - v_-(0)/\pi^{1/2} = (1 + \Delta p_\infty)/2,$$
$$Z_3 = -(\Delta n_-(0) + 3\Delta c_-(0)) + 5v_-(0)/4 = 5v_\infty/2.$$

The above equations are simultaneously solved and then we have

$$\begin{aligned} \Delta n_-(0) &= -18.79 v_\infty - 11.81 \Delta p_\infty, \\ \Delta c_-(0) &= -2.685 v_\infty - 1.686 \Delta p_\infty, \\ v_-(0) &= -15.18 v_\infty - 7.612 \Delta p_\infty, \\ (\text{or, } \Delta p_\infty &= -1.994 v_\infty - 0.1314 v_-(0)). \end{aligned} \tag{2.14}$$

It is assumed that $v_-(0)$ is nearly equal to v_∞. Then we can rewrite Eq. (2.14) in the following form:

$$v_\infty = \dot{m} = -0.470(p_\infty - 1). \tag{2.15}$$

That is, the condensation rate $\dot{m}$ depends on the pressure alone. Equation (2.15) is quite the same as the one obtained by Muratova and Labuntsov [5], Pao [6], Sone and Onishi [7] and Matsushita [8]. Using the relation (2.12) and (2.15), the macroscopic flow quantities are expressed as follows:

$$\begin{aligned} &n(0) = 1 + 0.630(1 + 1/\beta_l)(n_\infty - 1), \qquad v(0) = v_\infty, \\ &T(0) = 1 + 0.237(1 + \beta_l)(T_\infty - 1), \\ &p(0) = 1 + 0.867(p_\infty - 1), \qquad \dot{q}_y(0) = (0.572 - 0.178\beta_l)v_\infty(T_\infty - 1). \end{aligned} \tag{2.16}$$

As can be seen from Eq. (2.16), the flow quantities except $v(0)$ are proportional to $(n_\infty - 1)$, $(T_\infty - 1)$ and $(p_\infty - 1)$, respectively, and also proportional to $1/\beta_l$ or β_l. It should be noted that the relation $T(0) = T_\infty$ is obtained for the particular value of $\beta_l (= 3.22)$. In this case the temperature $T(y)$ is constant in the whole flow field and that $\dot{q}_y(y)$ is also zero in the whole flow field. Moreover, the flow field shows the peculiar flow pattern which is nearly uniform across the whole field when $\beta_l = 3.22$.

The value 3.22 of the parameter β_l nearly corresponds to the uniquely determined value of β_l for which the solution can be obtained by the ordinary linearized analyses [6–8]. It should be noted that it can be seen from Eq. (2.16) that the negative gradient of the temperature profile exists when $\beta_l > 3.22$.

III. Numerical Procedures

The straightforward computation is not necessarily feasible because the problem is the two-point boundary value one involving four unknown boundary values $n_-(0)$, $u_-(0)$, $v_-(0)$, $c_-(0)$. Since it is not at all practical to guess the four unknown boundary conditions at $y = 0$ directly and simultaneously, a set of alternate four quantities for easy guess should be picked up. In this paper, the conservation fluxes Z_0, Z_1, Z_2, Z_3 which appear in Eqs. (2.4–2.7) are selected. When a set of these flux $\boldsymbol{Z}$ is obtained, the remaining unknown boundary values can easly be derived by solving the conservation equations (2.4–2.7) simultaneously with the boundary conditions (2.8) and flow parameters. The schemes to make the proper guess for the conservation flux $\boldsymbol{Z}$ are obtained through the different manner for each configuration. Thus, with the aid of the initial guess of the conservation fluxes the present two point boundary value problem is reduced to the initial-value one.

For the Couette flow case, the solution of Lees [4] is made use of for the case of no evaporation. When the evaporation is extremely strong, the conseravation flux $\boldsymbol{Z}$ is easily derived; that is, $Z_0 = 1/(2\pi^{1/2})$, $Z_1 = 0$, $Z_2 = \pi^{1/2}/4$ and $Z_3 = 1$. For the intermediate value of the evaporation rate $\dot{m}$, linear relations among fluxes are found to be valid approximately by examining some numerical results under the conditions of the fixed temperature ratio T^* and the fixed Speed ratio S, and the existence of these relations is

proved in [*16*]. Using these approximate relations, the initial guess of the fluxes for the intermediate value of the evaporation rate is given by the following forms,

$$Z_0 = \dot{m}, \qquad Z_1 = (1 - 2\pi^{1/2} Z_0) Z_1',$$
$$Z_2 = Z_2' + (\pi - 4\pi^{1/2} Z_2') Z_0/2, \tag{3.1}$$
$$Z_3 = Z_3' - 2\pi^{1/2}(1 - Z_3') Z_0,$$

where Z_1', Z_2', Z_3' are the corresponding fluxes when $\dot{m}=0$. In Fig. 2, comparison between the initial guess by Eq. (3.1) and the numerical results are shown. The agreement with the initial guess is considered good. These relations make the numerical calculations very easy.

For the half space flow case, simple relations between conservation fluxes are analytically derived. Since the conservation equations (2.4–2.7) must asymptotically satisfy the boundary conditions (2.8) at infinity, then the conservation equations are rewritten in the following forms:

$$Z_0 = n_\infty v_\infty, \qquad Z_1 = n_\infty v_\infty S_\infty,$$
$$Z_2 = n_\infty T_\infty/2 + n_\infty v_\infty^2, \tag{3.2}$$
$$Z_3 = n_\infty v_\infty (5T_\infty/2 + S_\infty^2 + v_\infty^2).$$

In these relations the unknown variables are v_∞, Z_0, Z_1, Z_2 and Z_3. When one of these variables, for example v_∞, is suitably selected, the conservation fluxes are estimated correctly and simultaneously for the solution.

Using these conservation fluxes Z thus evaluated, the unknown boundary values $n_-(0)$, $u_-(0)$, $v_-(0)$ and $c_-(0)$ at the lower boundary are evaluated by applying the

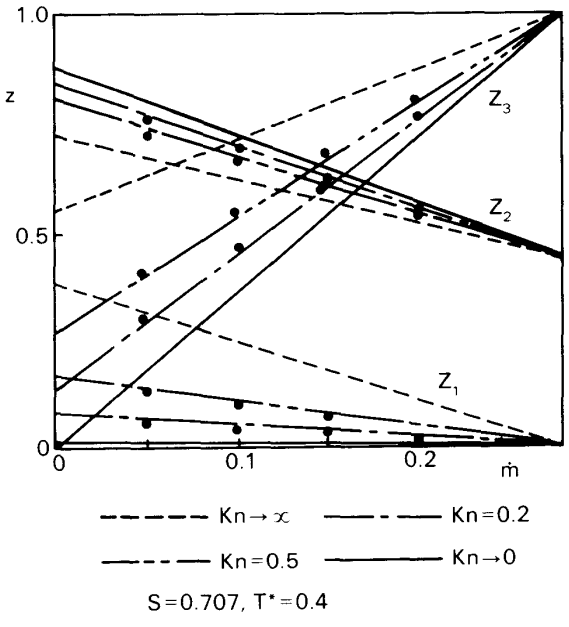

FIG. 2. Linear relation among fluxes for Couette flow case. $S=0.707$, $T^*=0.4$. (●; numerical results for $Kn=0.2, 0.5$)

boundary conditions (2.8) to the conservation equations (2.4–2.7). Thus the problem is reduced to the initial-value one. In fact, the solution for a set of moment equations can be easily achieved by numerical integration by menas of the Runge-Kutta-Gill method starting from the lower boundary at $y=0$ toward the upper boundary at $y=1$ (or $y\to\infty$).

When the numerical integration is performed up to the upper boundary, the set of the obtained values $\boldsymbol{F}(=(u_-(1), v_-(1), c_-(1))$ or $=(u_-(\infty), v_-(\infty), c_-(\infty))$ do not in general satisfy the boundary conditions $\boldsymbol{F}^{(b.c.)}(=(S, 0, T^*)$ or $=(S_\infty, v_\infty, T_\infty))$. In order to adjust $\boldsymbol{F}$ with $\boldsymbol{F}^{(b.c.)}$, the set of the initial guess of the conservation fluxes $\boldsymbol{Z}$ must be corrected. The scheme to correct $\boldsymbol{Z}$ to the suitable values is given by the following procedures; that is, the effects of the slight deviation of each conservation fluxes $\Delta\boldsymbol{Z}(\Delta Z_j, j=1-3)$ on $\boldsymbol{F}$ are estimated. These effects are expressed by a_{ij} $(=\Delta u_-/\Delta Z_j,\ \Delta v_-/\Delta Z_j,\ \Delta c_-/\Delta Z_j)$, where, Δu_-, Δv_- and Δc_- are the variations as the result of slight deviation of $\boldsymbol{Z}$. Then the corrections $\Delta\boldsymbol{Z}^c$ (or $\Delta\boldsymbol{Z}_j^c$) are given by solving the follwing equations with respect to ΔZ_j^c;

$$\boldsymbol{F}^{(b.c.)} = \boldsymbol{F} + \sum_j a_{ij}\Delta Z_j^c. \tag{3.3}$$

When the corrected values of $\boldsymbol{Z}$ are obtained, the numerical integration are performed and checked whether the new $\boldsymbol{F}$ coincides with $\boldsymbol{F}^{(b.c.)}$ or not. This numerical iteration procedures, which are often called the error propagation method, are repeated until $\boldsymbol{F}^{(b.c.)}$ is satisfied within the tolerance of a desired accuracy. The detailed scheme and of this procedure are shown in Ref. [16].

IV. Results and Discussion

A. *Examination of Choice of a Set of Moments*

The choice of higher-order generating functions such as V_y^2, V_y^3 except the collisional invariants is not unique, so that the deviation among the resulting solutions from possible choices of generating functions should be examined. Actually, for a few examples the examination was made. Liu and Lees [4] selected V_xV_y and V^2V_y for the higher-order generating functions together with four collisional invariants $(1, V_x, V_y, V^2)$. In the present problem, however, we need further two generating functions. Five set of additional generating functions (V_y^2, V_y^3), (V_x^2, V_y^3), (V_x^3, V_y^2), (V^2V_x, V_y^2), (V^2V_x, V_y^3) are chosen. It was confirmed that the results indicate only slight deviation among solutions so far as the criterion that provides "the higher priority to the lower order moment equations" is satisfied [16]. Actual computation was carried out by using the set (V_y^2, V_y^3) for the additional generating functions.

B. *Dependence of Condensation Rate on Specified External Conditions*

Since the simple analyses by Hertz [1] and Knudsen [2], it has been the important aim to estimate the condensation rate $\dot{m}$ under the specific circumstances; that is, under the specified flow parameters $(n_\infty, p_\infty, S_\infty)$ or $(\beta, p_\infty, S_\infty)$, where the parameter β is defined in Eq. (2.11).

First, we consider the cases of vanishing parallel velocity or $S_\infty=0$, in which the most of primary characteristics of condensation phenomena are retained. As for these cases,

the linearized analyses based on the BGK model equation provide the relation $\dot{m} = -0.470\,(p_\infty - 1)$ [6–8]. The similar relation is also derived from the linearized two-stream moment method by Muratova and Labuntsov [5]. However, in the non-linear flow regime the condensation rate $\dot{m}$ for the specified external flow parameters has not been estimated except a few numerical analyses [9, 10]. In the present analysis, therefore a systematic estimation of $\dot{m}$ for a wide variety of external flow parameters was carried out. The dependence of the mass flux rate on the external pressure is shown for various β in Fig. 3. It can be seen from this figure that for smaller condensation rates the relation of pressure versus condensation rate reduces to the one given by Eq. (2.15) regardless of any β, while for larger condensation rates this relation deviates largely from Eq. (2.15), depending also on the parameter β. This leads to the argument that the condensation rates depend, in general, on both p_∞ and n_∞ (or β), while for smaller condensation rates depend on p_∞ alone regardless of any number density n_∞ (or β).

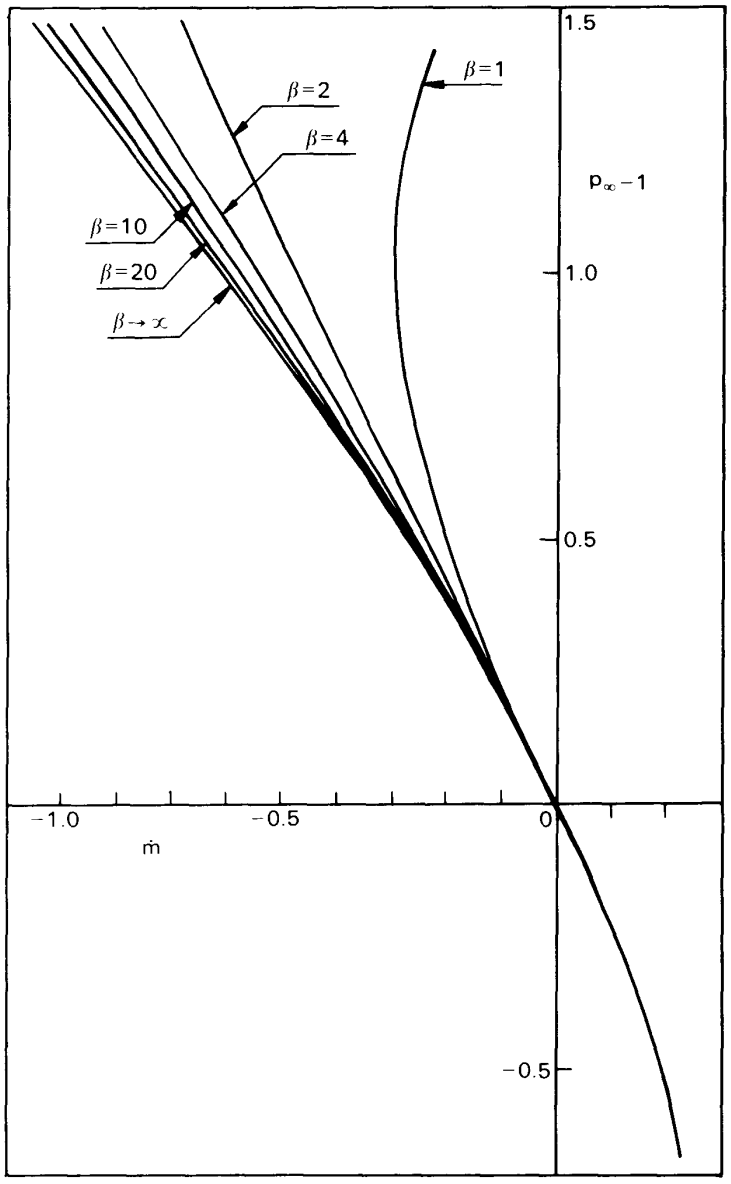

FIG. 3. Pressure at infinity versus mass flux rate $\dot{m}$. $S_\infty = 0$.

It should be noted that the similar dependence of $\dot{m}$ on p_∞ is also confirmed for smaller condensation rates by both the linearized analysis and the present non-linear analysis. The solution by the linearized analysis is valid only for a fixed value of $\beta(=4.66)$, while the solution by the non-linear analysis is obtained for any values of β. Muratova and Labuntsov [5] and Sone [15] dealt with the condensation processes taking into account non-linearity for cases of smaller condensation rates and pointed out that two external parameters (p_∞, β) need to obtain the flow field itself even for the smaller condensation rates and that the same relation as Eq. (2.15) is also valid. In what follows, we shall give a simple explanation for the aforementioned feature of the condensation. We pay the particular attention to the heat flux $\dot{q}_y(0)$. The heat flux has the second order of magnitude as is shown in the following:

$$\dot{q}_y(0) = 3v_\infty(T_\infty - T(0))/4. \tag{4.1}$$

In the linearized analysis $\dot{q}_y(y)$ is required to vanish in the whole flow field in order to satisfy the boundary conditions at infinity[5–8]. However, if the heat flux $\dot{q}_y$ is neglected, then a restrictive condition is naturally derived from Eq. (4.1) that the temperature $T(0)$ is equal to T_∞. This condition shows that $T(y)=T_\infty$ for any coordinate of y, and this is satisfied only when $\beta_l=3.22$ as already discussed in Chapter II [Eq. (2.16)]. The value 3.22 for β_l corresponds nearly to 4.66 for β. This result leads to the argument that if the heat flux $\dot{q}_y$ is formally neglected because of its smallness in the linearized flow analysis, a free parameter β_l is restricted to a fixed value: $\beta_l=3.22$. Therefore the half space flow with condensation is essentially the non-linear flow phenomena, and its non-linearity must be taken into account even in nearly equilibrium flow case. However, only when $\beta_l=3.22$ for the nearly equilibrium flow, the non-linear kinetic solution coincides with the linearized kinetic solution. The above explanation gives the reason why the linearized analysis is valid only when $\beta_l=3.22$.

The cases for evaporation ($\dot{m}>0$) are also calculated. The results are shown in Figs. 3 and 4. As can be seen from Fig. 3, the evaporation rate depends on the ambient pressure alone for any rate $\dot{m}$. This was previously pointed out in the references [9, 11 and 12]. The solution for evaporation can be achieved only for the specified values of the parameter β. These slightly decrease with increasing evaporation rate; for example, $\beta=4.48$ ($m\to 0$), $\beta=4.47$ ($\dot{m}=0.10$), $\beta=3.90$ ($\dot{m}=0.20$), and $\beta=3.34$ ($\dot{m}=0.23$). Moreover, the solution for evaporation can be achieved only for flows without the mean parallel velocity. Dependence of evaporation rate on n_∞ and T_∞ is shown in Fig. 4 in comparison with the results of previous works [9, 11, and 12].

C. *Structure of Non-linear Condensation Layer*

As mentioned in the introduction, only a few numerical analyses have been performed in the non-linear cases of the problem [9–15]. Therefore, it is of significance to clarify the flow fields for a wide variety of flow parameters and also the relevant characteristic structures of the non-linear condensation layer for the half space flow case. Several typical examples are presented for both larger $\dot{m}$ (4 cases) and smaller $\dot{m}$ (2 cases). Their profiles are shown in Figs. 5 and 7. These numerical examples were performed for the fixed value of p_∞.

In Fig. 5 shown are the density profile. As can be seen from the figure, the density n_0 of gases at the interphase is not necessarily smaller than the density n_∞ at infinity. It can be

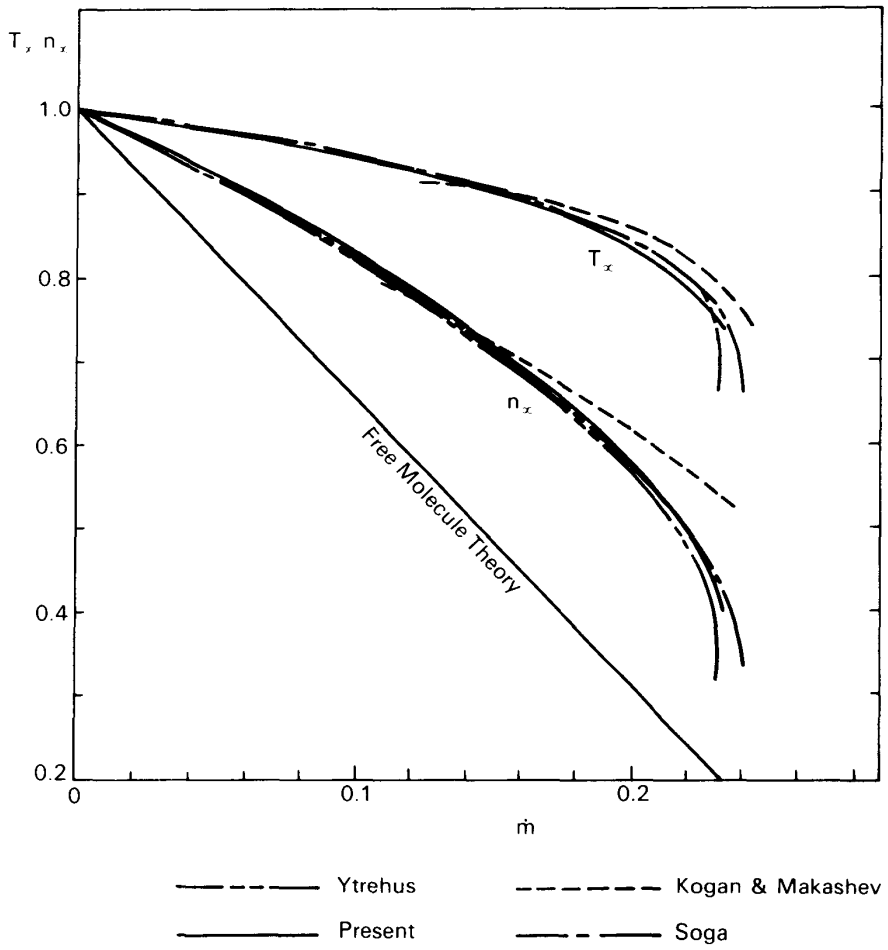

FIG. 4. Density and temperature at infinity versus evaporation rate.

said that the density profiles can be characterized by the ratio of the density difference $(n_\infty - n_0)$ to $(n_\infty - 1)$. In Fig. 6, the ratio $\bar{n}[=(n_\infty - n_0)/(n_\infty - 1)]$, is plotted versus $\dot{m}$ for various set of (β, T_∞) covering the ranges $2 \leqq \beta \leqq 10$ and $1.02 \leqq T_\infty \leqq 1.5$. In the figure, for the cases of constant β, $\bar{n}$ does not change so much. On the other hand, for the cases of constant T_∞, $\bar{n}$ changes greatly for smaller condensation rates, while $\bar{n}$ does not change for larger condensation rates. That is, the density profile which depends on $\bar{n}$ is roughly characterized by the parameter β.

In Fig. 7, the temperature profiles are shown. As can be seen from this figure, the profiles are rather monotonical so that the characteristics of temperature profile can be represented by the ratio of temperature difference $(T_\infty - T_0)$ to $(T_\infty - 1)$ for both linear and non-linear flow regimes. In Fig. 8, $\bar{T}[=(T_\infty - T_0)/(T_\infty - 1)]$ is plotted versus $\dot{m}$ for various set of (β, T_∞) covering the ranges $2 \leqq \beta \leqq 10$ and $1.02 \leqq T_\infty \leqq 1.8$. In the figure, for a case of fixed T_∞, $\bar{T}$ changes greatly for smaller condensation rates, while $\bar{T}$ does not change so much for larger condensation rates. It can be said from the figure that for $T_\infty s$ greater than roughly 1.10 or so, the temperature difference $(T_\infty - T_0)$ is always positive for any condensation rate, while for $T_\infty s$ smaller than roughly 1.10 or so, it changes the sign from positive to negative with increasing $\dot{m}$; in other words, the temperature gradient within the layer varies from positive to negative with increasing condensation rate $\dot{m}$. The occurrence of the negative temperature gradient can be identified in Fig. 8 when T_∞

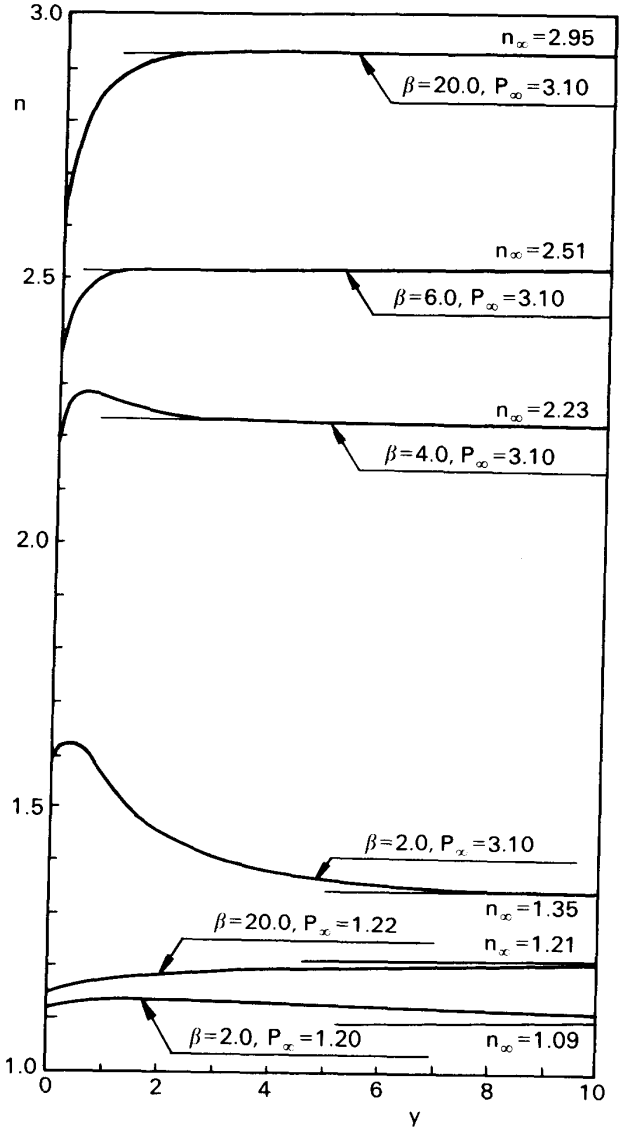

FIG. 5. Comparison of density profiles. $S_\infty = 0$.

and β are specified. Such a negative gradient of temperature profile has been pointed out by Pao [6], Matsushita [8] and Gajewski *et al.* [10] for cases of smaller temperature differences, while it was not shown in the results of the analysis by Kogan and Makashev [9] for cases of larger temperature differences. Therefore, it can be said that the present results are consistent with the previous results.

Moreover, it can be seen from Fig. 8 that for a certain value of β close to 4, the temperature difference or temperature profile does not indicate appreciable change for variation in T_∞ as well as $\dot{m}$. It should be noticing that this specific value of β is likely to be close to the one for which the solution can be obtined by the linearized analysis (or $\beta = 4.66$).

The other parameter characterizing the profile (or flow structure) is the one representing the layer thickness. By the definition similar to that of boundary layer thickness, we define a characteristic length L_T pertinent to temperature such that the temperature T_L at $y = L_T$ deviates from T_∞ by as much as 1%. In Fig. 9, the L_T defined

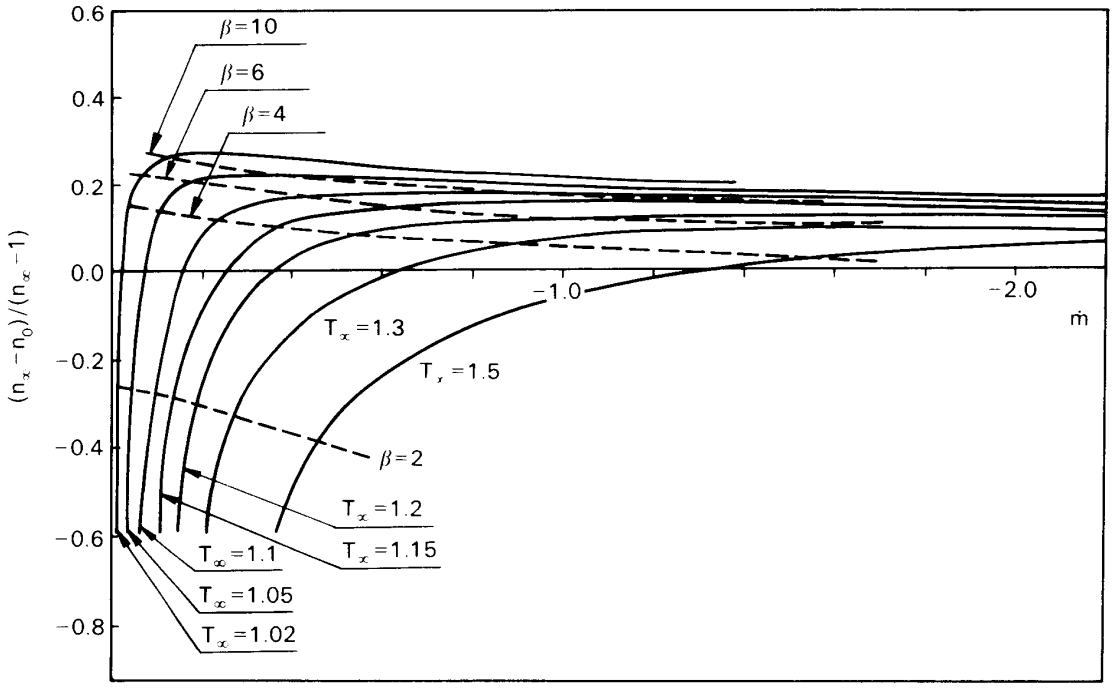

FIG. 6. $\bar{n}[=(n_\infty - n_0)/(n_\infty - 1)]$ versus $\dot{m}$ for various (β, T_∞) $S_\infty = 0$.

above is plotted against the condensation rate $\dot{m}$ for various T_∞ covering the range $1.02 \leq T_\infty \leq 1.2$. For T_∞ given, the temperature layer thickness L_T is likely to vanish at a certain value of $\dot{m}_{\min}$. In a region $\dot{m} < \dot{m}_{\min}$ the thickness increases sharply with decreasing condensation rate, while in a region $\dot{m} > \dot{m}_{\min}$, the thickness is likely to vanish again after slow increase with increasing condensation rate. Though the parameter β is not shown in the figure, it varies with $\dot{m}$ for a fixed T_∞. For the weak condensation case when T_∞ is close to unity, the β for which the L_T vanishes is found to be close to the particular value ($\beta = 4.66$), for which the solution can be achieved by the ordinary linearized analysis.

D. *Half Space Flow with Mean Parallel Velocity*

In this section, we consider the half space flow with condensation in the presence of the flow velocity $u(y)$ parallel to the wall. The condensation flow for the case of $S_\infty \neq 0$ is often observed in the actual condensation phenomena. In such a flow, it is natural that the structure of the flow field changes more or less. In authors' knowledge only the analysis by Kogan and Makashev [9] was carried out for a special Speed ratio S_∞ ($=0.5$).

In the present analysis, the flow parameters are $\beta = 2.0$, $T_\infty = 2.3$, ($p_\infty = 3.1$), and the Speed ratio is selected over a wide range $0 \leqq S_\infty \leqq 6$. In Fig. 10, condensation rate is plotted against the Speed ratio S_∞ for a set of fixed β and T_∞. In the figure, the condensation rate scarcely changes for smaller S_∞, while it indicates pronounced decrease with increasing S_∞ beyond unity or so. The condensation rate when $S_\infty = 6.0$ is about 1/3 of that when $S_\infty = 0$.

Next we consider the effect of S_∞ on the flow profiles. For $S_\infty \neq 0$, the distribution function $f_\pm$ shows the bimodal character by the presence of the parallel velocity $u_\pm(y)$ especially near the condensing surface, so that the presence of $u_\pm(y)$ directly affects the flow profiles. Since the definition of pressure is expressed by the second order moments

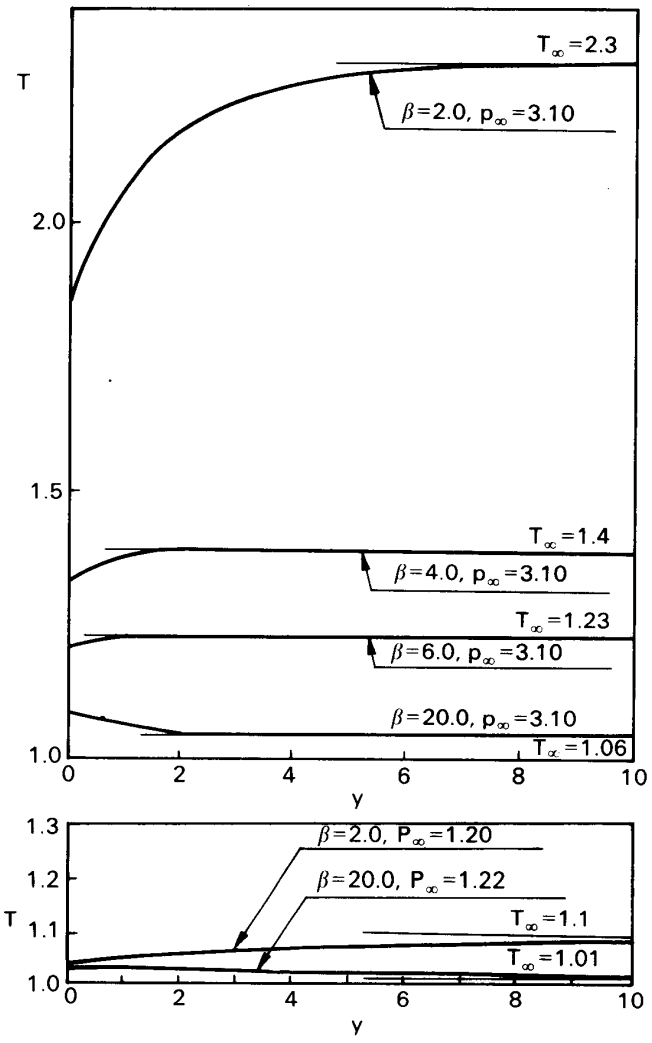

FIG. 7. Comparison of temperature profiles. $S_\infty = 0$.

around the mean velocity $\boldsymbol{u} = (u(\mathrm{y}), v(y), 0)$, the pressure increases as the bimodal character becomes stronger. The numerical results are presented in Fig. 11. In the figure the pressure profiles for the cases $S_\infty = 0$, 2.0, and 4.0 are shown. The increase of pressure is remarkable especially near the condensing surface. Thus, $p(0)/p_\infty$ is plotted versus S_∞ in Fig. 12. In the figure, the $p(0)$ is higher than p_∞ by about 40% when $S_\infty = 6.0$. The occurrence of this high pressure near the condensing wall is considered to be one of the causes which prevent the vapor from coming onto the interphase.

The effect of the parallel velocity on the temperature profiles is shown in Fig. 13. The temperature increases greatly as S_∞ increases in the whole region of the flow field. The tendency becomes clearer by illustrating the $T(0)/T_\infty$ versus S_∞, which is shown in Fig. 14. As is clearly observed in the figure, the presence of the parallel velocity affects greatly the condensation rate and the structure of the flow field. Such a great change of the flow field causes the change of the temperature layer thickness L_T and of the parallel velocity layer thickness L_u. The definition of the parallel velocity layer thickness L_u is quite the same as that for the temperature layer thickness L_T.

The L_T and L_u are summarized in Fig. 15. Both L_T and L_u are nearly the same in magnitude and show a slow increase for smaller S_∞ and a sharp increase for larger S_∞

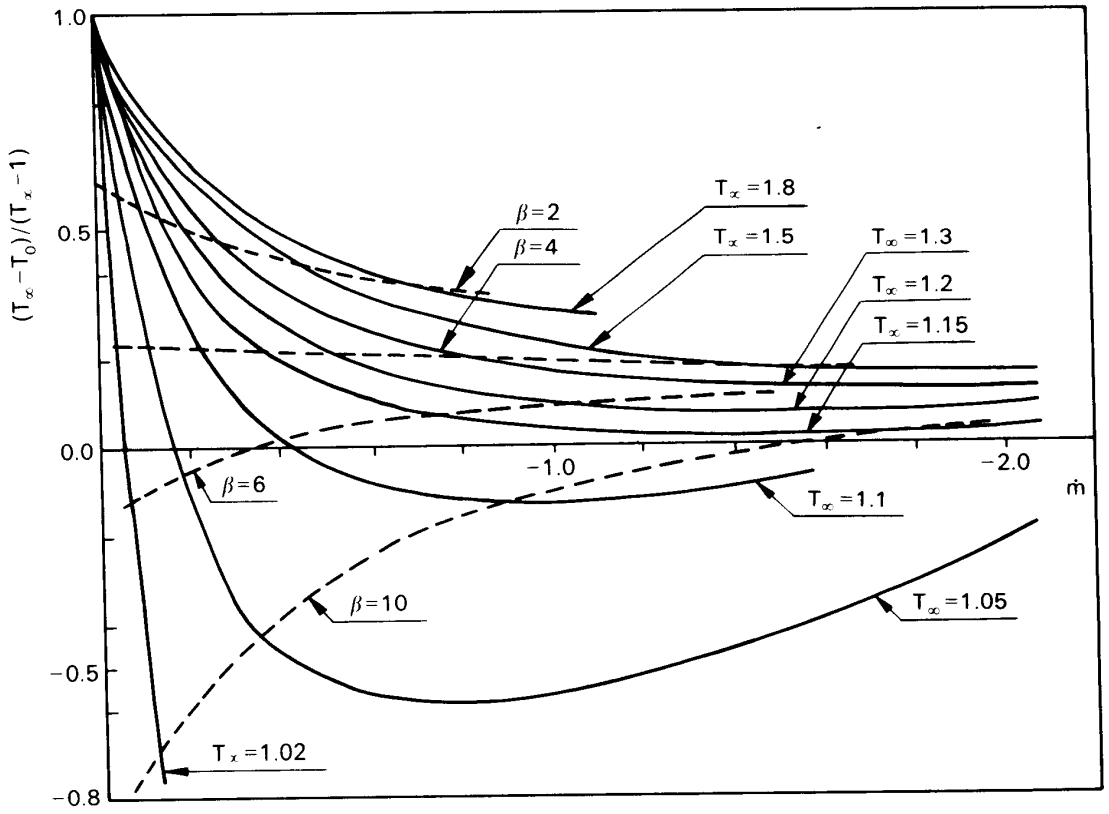

FIG. 8. $\bar{T}[=(T_\infty - T_0)/(T_\infty - 1)]$ versus $\dot{m}$ for various (β, T_∞). $S_\infty = 0$.

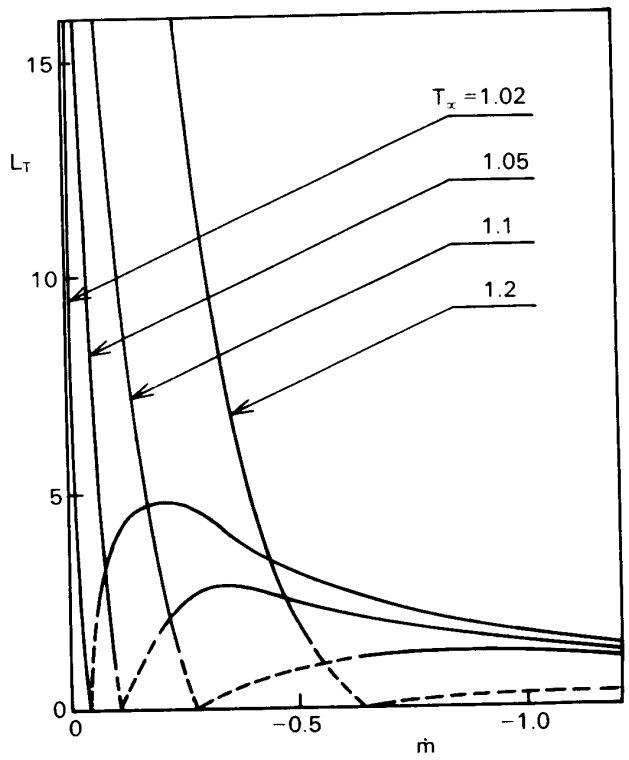

FIG. 9. Temperature layer thickness L_T versus $\dot{m}$ for various T_∞. $S_\infty = 0$.

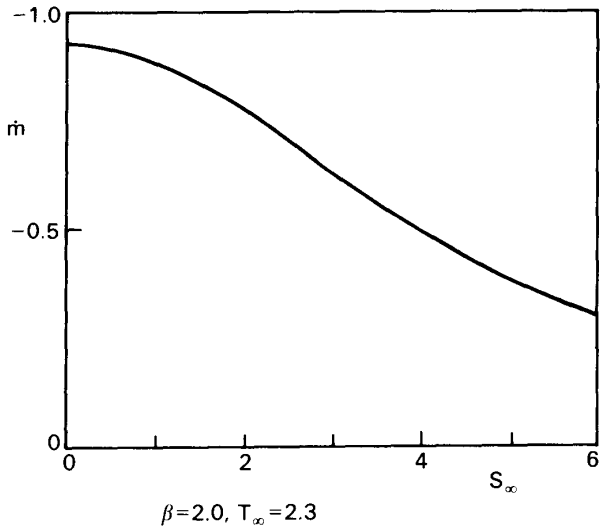

FIG. 10. Effect of parallel velocity S_∞ on condensation rate $\dot{m}$. $\beta=2.0$, $T_\infty=2.3$.

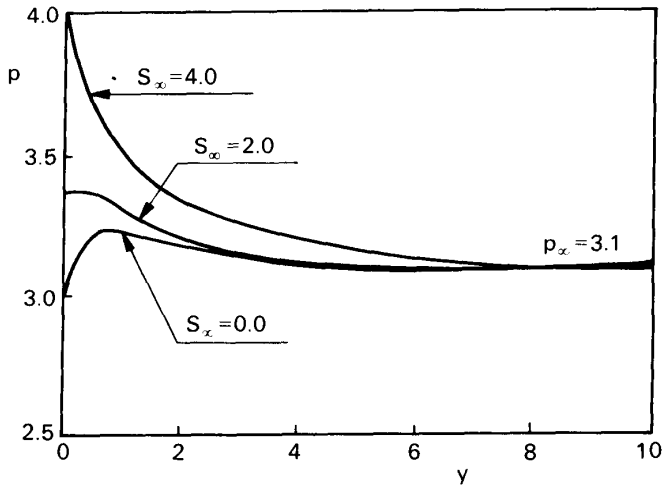

FIG. 11. Comparison of pressure profiles for various S_∞. $\beta=2.0$, $T_\infty=2.3$.

beyond unity or so. To observe the whole flow field for the case $S_\infty=4.0$, the flow profiles are presented in Fig. 16.

E. Couette Flow with Evaporation and Condensation

We consider the Couette flow with evaporation and condensation through the both interphases at $y=0$ and $y=1$ as is illustrated in Fig. 1. The aims are to clarify the differences of flow profiles between the cases with and without evaporation and condensation, and to present some numerical examples for the case with the mean parallel valocity, which have scarcely been presented except a few numerical examples by Makashev [*13*].

In Figs. 17–19, the flow profiles are presented for the case when $Kn=0.2$, $S=0.707$, and $T^*=0.7$. The mass flux $\dot{m}$ is selected as the flow parameter instead of the parameter β. Four kinds of mass flux rate (evaporation rate) are taken: 0.0, 0.05, 0.10, 0.15. The attainable evaporation rate is $1/2\pi^{1/2}$ ($=0.282$). The corresponding values of β are 0.73 (for $\dot{m}=0.05$), 1.40 (for $\dot{m}=0.10$), and 2.33 (for $\dot{m}=0.15$).

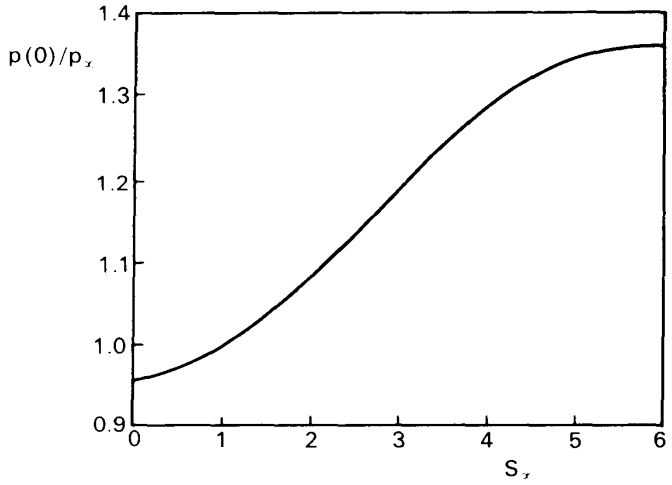

FIG. 12. Effect of parallel velocity S_∞ on Pressure $p(0)$. $\beta=2.0$, $T_\infty=2.3$.

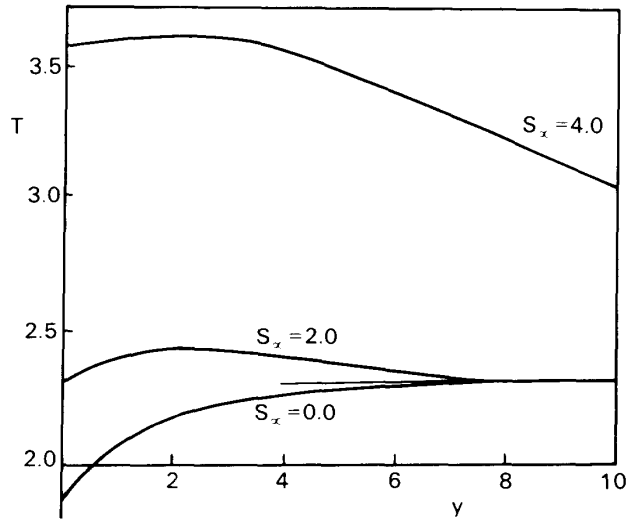

FIG. 13. Comparison of temperature profiles for various S_∞. $\beta=2.0$, $T_\infty=2.3$.

The density profiles $n(y)$ are presented in Fig. 17. In the figure, two characteristics are observed when compared the cases $\dot{m}\neq 0$ with the case $\dot{m}=0$. One is that the density for the case of larger mass flux is lower over the whole region than the case with smaller or zero mass flux. It is due to the lower number density of the saturated vapor at the condensing surface for the cases of $\dot{m}\neq 0$ in comparison with that when $\dot{m}=0$. The other characteristic is that the gradients of the profiles near the both boundaries for the cases $\dot{m}\geqq 0.10$ are contrary to those for the case $\dot{m}\leqq 0.05$.

In Fig. 18, the parallel velocity profiles are presented. The parallel velocity for larger mass flux is lower over the whole region than that for smaller or zero mass flux. This suggests that the influence of the condensing wall with the parallel velocity on the flow field becomes smaller with increasing the mass flux. In Fig. 19, the temperature profiles are presented. The temperature decreases monotonically with approaching the condensing surface. It should be noted that with increasing mass flux the variation in temperature becomes much slower.

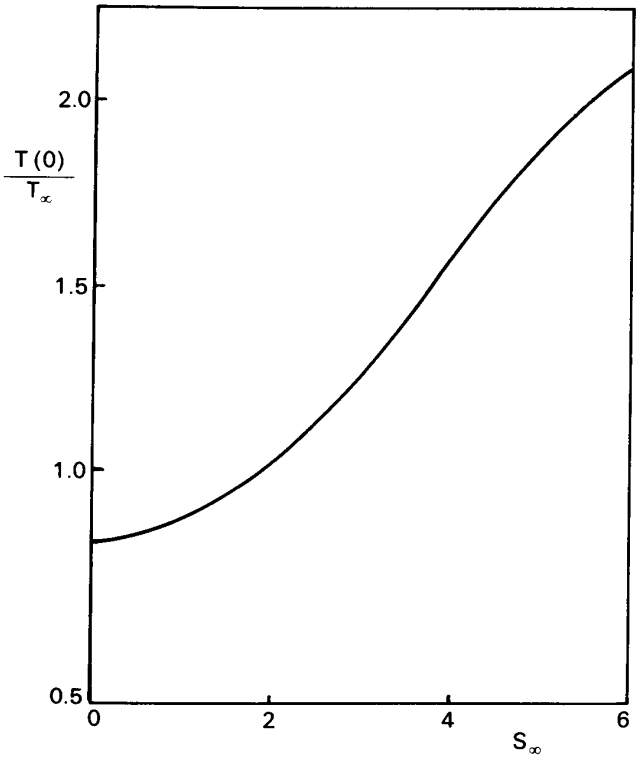

FIG. 14. Effect of parallel velocity S_∞ on temperature $T(0)$. $\beta=2.0$, $T_\infty=2.3$.

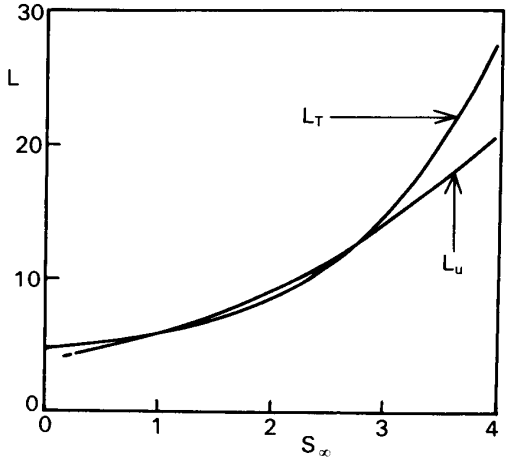

FIG. 15. Effect of parallel velocity S_∞ on layer thickness L_T and L_u. $\beta=2.0$, $T_\infty=2.3$.

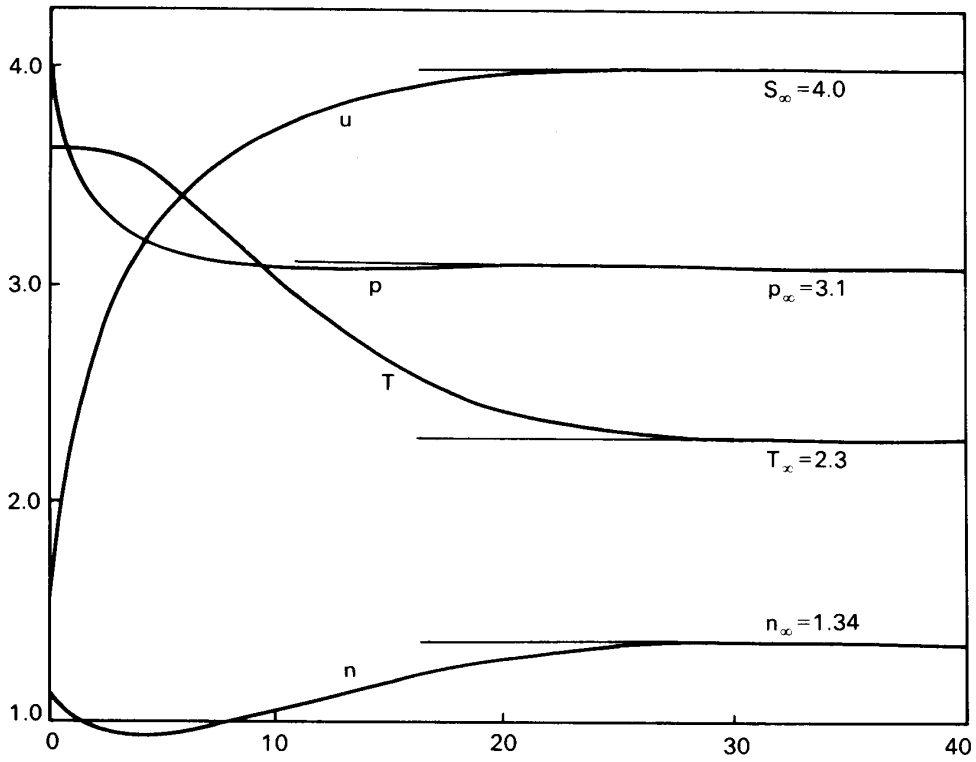

FIG. 16. Flow profiles with condensation for $S_\infty=4.0$. $\beta=2.0$, $T_\infty=2.3$.

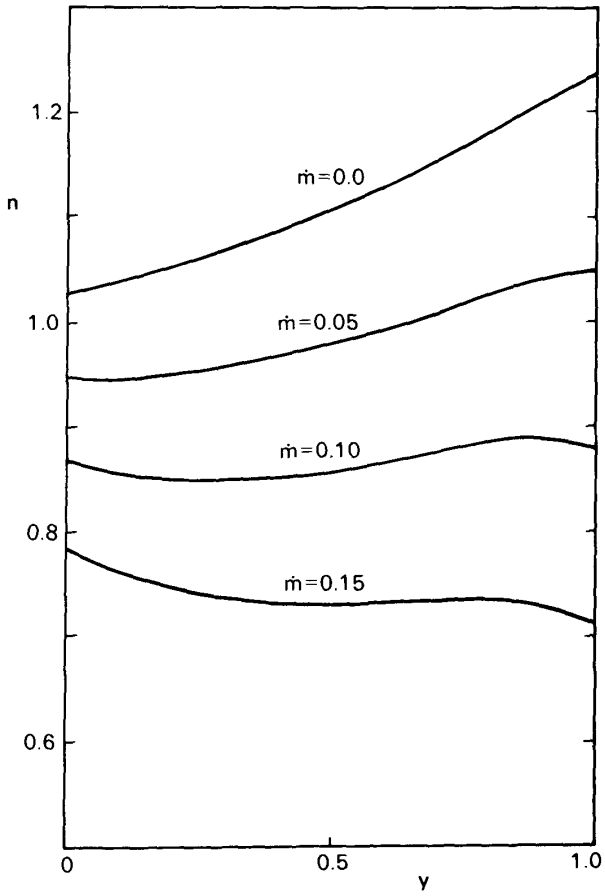

FIG. 17. Comparison of density profiles for Couette flow. $Kn=0.2$, $S=0.707$, $T^*=0.7$.

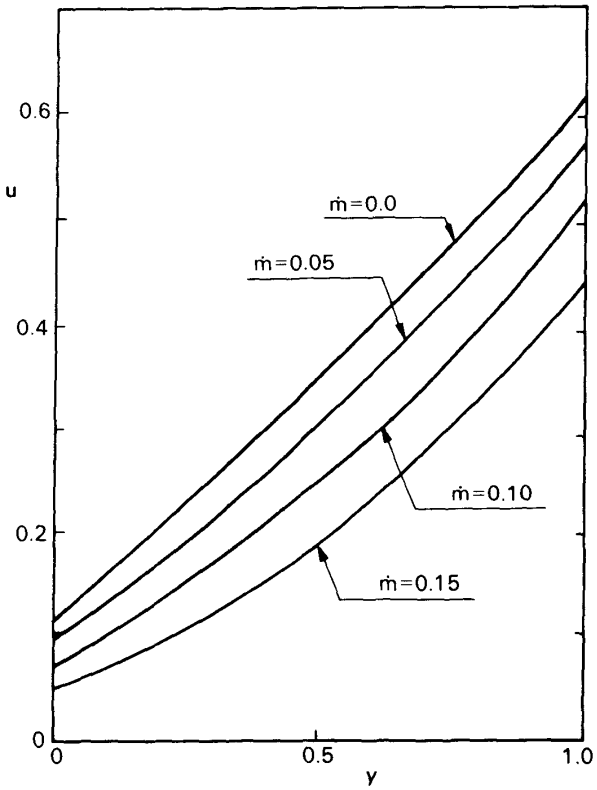

FIG. 18. Comparison of parallel velocity profiles for Couette flow. $Kn=0.2$, $S=0.707$, $T^*=0.7$.

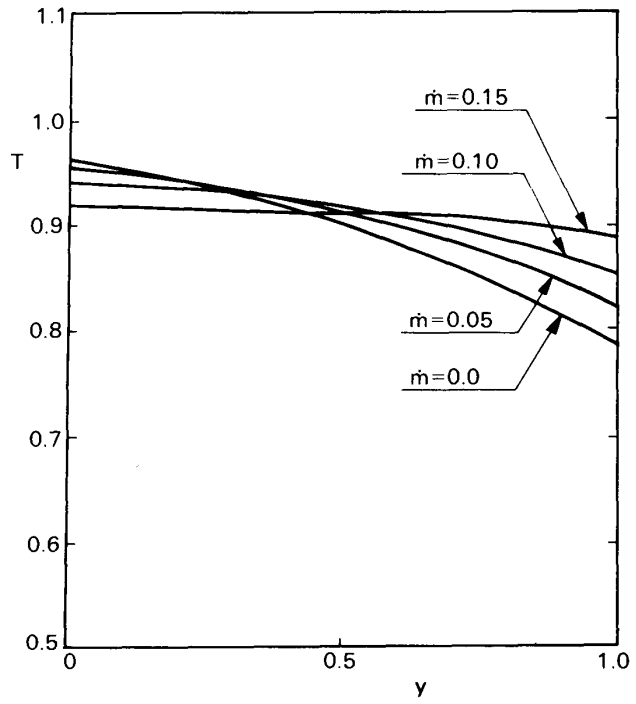

FIG. 19. Comparison of temperature profiles for Couette flow. $Kn=0.2$, $S=0.707$, $T^*=0.7$.

Department of Aerodynamics
Institute of Space and Aeronautical Science
University of Tokyo
May 11, 1979

REFERENCES

[1] H. Hertz, Ann. Physik, 17, 177 (1882).
[2] M. Knudsen, Ann. Physik, 47, 697 (1915).
[3] R. W. Schrage, Columbia Univ. Press, New-York, (1953).
[4] C. Y. Liu and L., Lees, in *Rarefied Gas Dynamics,* L. Talbot, Ed. (Academic Press, New-York, 1961) Suppl. I, 391.
[5] T. M. Muratova and D. A. Labuntsov, High Temperature, 7, 888 (1970).
[6] Y. P. Pao, Phys. Fluids, 14, 306 (1971).
[7] Y. Sone and Y. Onishi, J. Phys. Soc. Japan, 35, 1773 (1973).
[8] T. Matsushita, ISAS Rep. 541, Univ. Tokyo (1976).
[9] M. N. Kogan and N. K., Makashev, Fluid Dynamics, 6, 913 (1974).
[10] P. Gajewski, A. Kliski, A. Wiswieniski and M. Zgorzeiski, Phys. Fluids, 17, 321 (1974).
[11] T. Ytrehus, von-Karman Institute, Fluid Dynamics Div. T. N. No. 112, (1975).
[12] T. Soga, in *Rarefied Gas Dynamics,* Progress in Astro. and Aero., J. L. Potter, Ed., (AIAA, New-York, 1977) Vol. 51, Part II, 1185.
[13] N. K. Makashev, Fluid Dynamics, 7, 815 (1974).
[14] S. M. Yen, in *Rarefied Gas Dynamics,* M. Becker and M. Fiebig, Eds., 1, A-15 (1974).
[15] Y. Sone, J. Phys. Soc. Japan, 45, 315 (1978).
[16] M. Hatakeyama, Memo. Tokyo Metro. College Aeron. Eng., Vol. 16, 69 (1979).

APPENDIX

$$K^{(0)} = \frac{1}{2}(1 + \operatorname{erf}(w_+)),$$

$$L^{(0)} = \frac{1}{2}(1 - \operatorname{erf}(w_-)),$$

$$K^{(1)} = \frac{1}{2}w_+(1 + \operatorname{erf}(w_+)) + \frac{1}{2\sqrt{\pi}}\exp(-w_+^2),$$

$$L^{(1)} = \frac{1}{2}w_-(1 - \operatorname{erf}(w_-)) - \frac{1}{2\sqrt{\pi}}\exp(-w_-^2),$$

$$K^{(2)} = \frac{1}{4}(2w_+^2 + 1)(1 + \operatorname{erf}(w_+)) + \frac{w_+}{2\sqrt{\pi}}\exp(-w_+^2),$$

$$L^{(2)} = \frac{1}{4}(2w_-^2 + 1)(1 - \operatorname{erf}(w_-)) - \frac{w_-}{2\sqrt{\pi}}\exp(-w_-^2),$$

$$K^{(3)} = \frac{1}{2}w_+\left(w_+^2 + \frac{3}{2}\right)(1 + \operatorname{erf}(w_+)) + \frac{1}{2\sqrt{\pi}}(w_+^2 + 1)\exp(-w_+^2),$$

$$L^{(3)} = \frac{1}{2}w_-\left(w_-^2 + \frac{3}{2}\right)(1 - \operatorname{erf}(w_-)) - \frac{1}{2\sqrt{\pi}}(w_-^2 + 1)\exp(-w_-^2),$$

$$K^{(4)} = \frac{1}{8}(4w_+^4 + 12w_+^2 + 3)(1 + \operatorname{erf}(w_+)) + \frac{1}{4\sqrt{\pi}}(2w_+^3 + 5w_+)\exp(-w_+^2),$$

$$L^{(4)} = \frac{1}{8}(4w_-^4 + 12w_-^2 + 3)(1 - \operatorname{erf}(w_-)) - \frac{1}{4\sqrt{\pi}}(2w_-^3 + 5w_-)\exp(-w_-^2),$$

where $w_\pm = v_\pm/c_\pm$.